Title: STRUCTURES OF MESOPHILIC AND EXTREMOPHILIC CITRATE SYNTHASES REVEAL RIGIDITY AND FLEXIBILITY FOR FUNCTION

Short Title: RIGIDITY AND FLEXIBILITY IN CITRATE SYNTHASES

Key words: Rigidity, flexible motion, geometric simulation, elastic network, FIRST, FRODA, Elnemo, thermophile, psychrophile

[1]Stephen A. Wells, [2]Susan J. Crennell and [2]Michael J. Danson

[1]Department of Physics, University of Bath, BATH BA2 7AY, UK.

[2]Centre for Extremophile Research, Department of Biology and Biochemistry, University of Bath, BATH BA2 7AY, UK.

Contact: Dr. Stephen A. Wells, tel: 01225 386645, email: s.a.wells@bath.ac.uk

ABSTRACT

Citrate synthase (CS) catalyses the entry of carbon into the citric acid cycle and is highly-conserved structurally across the tree of life. Crystal structures of dimeric CSs are known in both "open" and "closed" forms, which differ by a substantial domain motion that closes the substrate-binding clefts. We explore both the static rigidity and the dynamic flexibility of CS structures from mesophilic and extremophilic organisms from all three evolutionary domains. The computational expense of this wide-ranging exploration is kept to a minimum by the use of rigidity analysis and rapid all-atom simulations of flexible motion, combining geometric simulation and elastic network modelling. CS structures from thermophiles display increased structural rigidity compared with the mesophilic enzyme. A CS structure from a psychrophile, stabilised by strong ionic interactions, appears to display likewise increased rigidity in conventional rigidity analysis; however, a novel modified analysis, taking into account the weakening of the hydrophobic effect at low temperatures, shows a more appropriate decreased rigidity. These rigidity variations do not, however, affect the character of the flexible dynamics, which are well conserved across all the structures studied. Simulation trajectories not only duplicate the crystallographically observed symmetric open-to-closed transitions, but also identify motions describing a previously unidentified antisymmetric functional motion. This antisymmetric motion would not be directly observed in crystallography but is revealed as an intrinsic property of the CS structure by modelling of flexible motion.

INTRODUCTION

Citrate synthase (CS; EC 2.3.3.1) occurs in almost all organisms and is highly-conserved structurally across the tree of life. It catalyses the entry of carbon, in the form of acetyl-CoA, into the citric acid cycle:

$$\text{Acetyl-CoA} + \text{Oxaloacetate} + H_2O \longrightarrow \text{Citrate} + \text{CoA}$$

The enzyme has a characteristic dimeric structure; each subunit displays a large and a small domain, with the main body of the dimer being formed by the association of the large domains. The structure of the dimer is shown in Figure 1A. The cleft between the large and small domain on each subunit forms an active site, which binds oxaloacetate first, followed by acetyl-CoA, leading to the formation of citrate. A substantial motion of the small domain relative to the large domain, closing and opening the cleft, is involved in this function. The extent of cleft opening varies widely between the different structures and there has been debate as to whether this is linked to thermostability. Normal mode analysis has suggested that the crystallographically-observed symmetric opening and closing motion is a natural low-frequency flexible motion of the CS structure [1-3].

In extremophilic organisms, the structure and function of proteins must be maintained in the face of challenges such as high or low temperatures (thermophiles and psychrophiles, respectively), high salinity (halophiles) or extremes of pH (acidophiles and alkalophiles) that would rapidly denature and deactivate proteins from mesophilic organisms [4]. The nature of the mutations involved in thermoadaptation of enzymes has been the subject of detailed structural and experimental investigation (e.g. [5,6]). In the case of proteins from thermophiles, a variety of covalent and non-covalent interactions have been identified that provide greater structural rigidity, which favours thermostability [7,8]. However, for a protein such as CS whose

function requires large-scale flexible motion, there would appear to be a tension between the need to stabilise the structure of the protein, and the need to maintain function – that is, between rigidity and flexibility.

The gold standard in the atomistic simulation of motion in proteins is generally considered to be empirical-potential molecular dynamics (MD) and molecular mechanics (MM). With modern high-performance computing resources MD can be applied to study the motion of large biomolecular systems [9] and MM can be combined with quantum mechanical simulation methods, e.g. in QM/MM embedding schemes [10], to study bonding and chemical reactions. Extending these methods to long biological timescales and large amplitudes of motion is, however, very demanding in computational resources. Previous MD studies on citrate synthases have tended to use short trajectories on the order of 1-2ns [11-13]. A common approach to accelerate MD is the use of a coarse-graining scheme [14], sacrificing a certain amount of steric detail in order to reduce the number of interacting bodies in the simulation [15,16].

A parallel approach is to retain full atomistic detail in the structure but to simplify the physical model with which motion is investigated. In this work we explore experimental crystal structure data for CS from multiple extremophilic and mesophilic organisms using rigidity analysis [17-19], normal mode analysis [20], and geometric simulation of flexible motion [21,22]. All the structures used in our analysis are listed in Table I and are described further in the Methods section. We label our structures with a prefix for the organism and a postfix for the ligand-binding state, thus TtCS-0 labels a CS structure from *Thermus thermophilus* with no ligands bound in the cleft. Geometric simulations can project an all-atom model of a protein structure over large distances at minimal computational expense [22-25]. Thus, we can

explore large amplitudes of flexible motion in multiple structures in parallel. The geometric model retains the bonding geometry and non-covalent interaction network of the input structure, and maintains steric exclusion. Recent studies have shown that these simulations are sufficiently realistic to be used in the interpretation of experimental data [26,27].

In the current paper, we compare our simulations of closing motion to experimental crystal structures of CS in its closed conformation. We obtain intriguing information on the rigidity and flexibility of CS, the significance of multiple normal modes for CS function, the conservation of flexible behaviour linked to catalytic function in CS, and the capacity of structures to open and close further than is crystallographically observed. These results highlight the value of modelling in bringing out the information on flexibility and mobility that is implicit in protein crystal structures.

EXPERIMENTAL PROCEDURES (METHODS)

Structure selection

Citrate synthase (CS) structures were considered from a "reference" mesophilic metazoan, the pig (*Sus scrofa*), the mesophilic *Bacillus subtilis* and from a range of microorganisms, principally extremophilic: *Thermus thermophilus, Thermoplasma acidophilum, Sulfolobus solfataricus, Pyrobaculum aerophilum, Pyrococcus furiosus,* and the Antarctic bacterium *Arthrobacter* DS2-3r. Structures are referred to by a prefix describing the organism, (e.g. Ta for *T. acidophilum*), and by a suffix describing the number of ligands resolved in each binding cleft. Thus -0 indicates an unliganded structure, -1 indicates a single ligand bound (e.g. oxaloacetate) and -2 indicates a structure with both coenzyme A and citrate ligands bound. For example, TaCS-0 indicates an unliganded CS structure from *T. acidophilum*. In general, doubly ligand-bound structures can be considered closed while unliganded structures are open. An exception is the *B. subtilis* structure (BsCS-2, PDB code 2C6X), which was crystallised in the presence of citrate and coenzyme A ligands, but is found to be in a fully open state as the ligands are not bound in a functional position in the cleft. PDB codes and resolutions for our set of structures are given in Table I.

(Table I)

From the PDB entry for each structure, a model of the dimeric CS structure showing all heavy atoms was obtained. Heteroatoms, including water molecules, ligands and ions, were removed and hydrogens added to the structure using the MolProbity "Reduce" function [28], to obtain a structure suitable for rigidity analysis and flexible motion simulation.

For rigidity analysis, only those sets of structures with resolutions of 2.0 Å or better were

examined, while for flexible motion a set of "open" structures were considered.

Rigidity analysis

Rigidity analysis was carried out using the "pebble game" algorithm implemented in FIRST [18], which matches degrees of freedom against constraints in a molecular framework, to divide a structure into rigid clusters and flexible regions. Rigid cluster decomposition (RCD) assigns each atom to membership in a rigid cluster (RC) with an index *j*, with RC_1 being the largest cluster. For comparison of rigidity results between different structures, it is informative to consider the cumulative rigidity fraction, f_i, which measures the fraction of the α-carbons of the structure lying within clusters $RC_{1,2}$... up to RC_i.

The key control parameter is an "energy cut-off" (E_{cut}), which selects the set of polar interactions to be included as constraints [17]. Only interactions whose bond energy is calculated (based on their geometry) to be less than the cut-off are included. Of particular consideration was the variation in rigidity as E_{cut} is tuned from near zero, where the structure is largely rigid due to the inclusion of many weak bonds, to around -4 kcal/mol, where only the strongest hydrogen bonds and salt bridges are included and the structure is largely flexible. In this analysis, steps of 0.5 kcal/mol in E_{cut} were taken. For rigidity analysis, structures with a resolution of around 2.0 Å or better were focussed on to ensure the reliability and consistency of results [19].

For the case of psychrophilic AbCS-2, it was necessary to modify the handling of hydrophobic tether interactions, to model the weakening of the hydrophobic interaction at low temperatures. By default a hydrophobic tether interaction introduces two constraints in rigidity analysis (for comparison, a typical covalent bond introduces five). A modified listing

of hydrophobic tethers was prepared in which each such interaction introduced only one constraint. This modification gave satisfactory results for AbCS-2 and may be of general use for rigidity analysis on protein structures from psychrophilic organisms.

Normal modes

Low-frequency normal modes were identified using a coarse-grained elastic network model as implemented in the "Elnemo" software [3,20]. The structure is represented as one site for each residue, using the C-α geometry; springs of equal strength are placed between all sites lying within a distance cut-off of 12 Å. Construction and diagonalisation of the interaction matrix (3Nx3N for a protein of N residues), using the Elnemo "pdbmat" and "diagstd" utilities, produces a set of 3N normal modes, of which the first six are trivial combinations of rigid-body displacements and rotations. Focus was placed on the lowest-frequency non-trivial modes. Since motion along these directions incurs little or no restoring force, these are the motions that the structure will most easily explore when driven by impulses from the surrounding solvent. This study focused on the three lowest-frequency non-trivial modes, modes 7, 8 and 9, which describe collective motions of the entire protein structure, particularly the motions of the two small domains relative to the main body of the dimer. Higher modes are more localised.

Geometric simulation

Motion of the all-atom protein structure was explored in the direction of normal mode eigenvectors using template-based geometric simulation [21] implemented in the FRODA module of FIRST. This approach uses a simplified physical model including local steric exclusion, local non-covalent distance constraints (polar and hydrophobic interactions as identified by FIRST) and covalent-bonding geometry represented by an overlapping network

of templates. Weaker long-range interactions are neglected. New conformations of the protein are generated by an iterative process in which all atomic positions are slightly perturbed and then relaxed to satisfy distance and bonding constraints. By perturbation parallel or antiparallel to a normal mode eigenvector [22], substantial amplitudes of flexible motion can be explored at minimal computational cost.

This exploration of flexible motion typically shows an early phase of "easy" motion in which new conformations are generated rapidly and all constraints are easily satisfied, and a later phase in which constraints begin to be violated (e.g. serious steric overlaps, over extension of hydrophobic tethers) and the generation of new conformations slows considerably. Focus was on motion within the "easy" phase. In this study, several thousand cycles of perturbation and relaxation for each direction of motion were performed, saving conformations every 100 or 200 cycles. This produces a series of "frames" separated by some tenths of an Angstrom in RMSD and typically explores a total RMSD of several Angstroms of "easy" flexible motion.

Simulations were carried out using the constraint networks obtained from rigidity analysis with cut-off energies of -2.0, -3.0 and -4.0 kcal/mol, in line with other studies [26,27]. The motions along these lowest-frequency modes were essentially identical at these cut-offs. Mobility data are shown for a cut-off of -3.0 kcal/mol in all cases.

Visualisation

Structures have been visualised using PyMOL [29] and graphs were prepared using gnuplot.

RESULTS AND DISCUSSION

Rigidity analysis

Rigidity analysis considers the protein as a constraint network that can be divided into rigid and flexible regions. The results depend on the set of bonds that are included as constraints in the network. While covalent and hydrophobic interactions are always included, the inclusion of polar interactions can be controlled using an energy cut-off parameter which excludes weaker interactions (i.e. hydrogen bonds with poor geometry) from the network [17]. By progressively lowering this cut-off parameter, comparative information on the relative rigidity of different protein structures and parts of structures is obtained. Previous studies have suggested that in thermostable proteins from extremophilic organisms, the "folding core" of the protein is stable to lower hydrogen-bond cut-off energies than in proteins from mesophiles[7]; and that the rigidity of enzymes from mesophilic and thermophilic organisms conforms to the hypothesis of corresponding states, with the rigidity of extremophilic enzymes at high temperatures being comparable to that of mesophilic enzymes at room temperature[8]. Here the rigidity of a selection of dimeric CS crystal structures has been examined, making use of a "rigidity fraction" measure (as discussed in Methods) that tracks the loss of rigidity in the entire structure as weaker interactions are removed from the constraint network [19]. We have focussed on structures with the best available resolution, as the results of rigidity analysis depend sensitively on the accuracy of the atomic geometry in the input structure.

(Fig1)

Figure 1 shows rigid cluster decompositions for open CS structures from a mesophile, pig

(PigCS-0, Figure 1A,C,E), and a thermophile, *Thermus* (TtCS-0, Figure 1B,D,F), with the cut-off energy for hydrogen bond inclusion set to 0.0 kcal/mol, -1.0 kcal/mol and -2.0 kcal/mol respectively. These bond strengths can be compared to temperature by noting that the gas constant $R = 1.99\times10^{-3}$ kcal/(K mol), so that RT at room temperature is approximately 0.6 kcal/mol. As the cut-off is lowered, more and more of the structure becomes flexible and a smaller fraction of the structure lies within a large rigid cluster. With a cut-off of 0.0 kcal/mol, including even very weak bonds in the analysis, both structures are entirely rigid, while at -2.0 kcal/mol both structures show considerable flexibility. At the cut-off of -1.0 kcal/mol, however, there is a clear difference between PigCS-0, where the small domains are already flexible, and TtCS-0, where the small domains are still rigid relative to the body of the dimer. These constraints would greatly reduce the capacity of the extremophile structure to carry out functional motion at room temperature.

Figure 1G illustrates the different behaviour of CS structures from pig and *Thermus* during such a rigidity dilution, using the rigidity fraction *f(i)* of C-α atoms lying in the *i* largest rigid clusters, as a function of cut-off energy and *i*. In particular, for cut-off energies of -0.5 and -1.0 kcal/mol (i.e. around the room temperature range) the pig structure already displays substantial flexibility, while the *Thermus* structure remains largely rigid, with almost all the protein lying within a single large rigid cluster. Figure 1H compares this type of rigidity information, using the *f(5)* measure, the fraction of the backbone lying within the five largest rigid clusters, for CS structures from pig (mesophile) and multiple extremophiles. The enhanced rigidity for all the thermophiles in the -0.5 to -1.0 kcal/mol cut-off range is consistent and clear. This appears to be the signature of a stronger network of polar interactions stabilising the extremophile structures [4,5,30].

Previous studies on thermostabilisation and rigidity analysis have considered protein structures from mesophiles and thermophiles [7,8]; we go on to consider cold-adaptation in a psychrophile. The Antarctic *Arthobacter* CS structure, AbCS-2, is an interesting case. It has been previously noted [31] that this structure contains an unusually large number of intramolecular ion pairs, possibly to counteract the reduced thermodynamic stabilisation due to hydrophobic interactions at low temperatures. These strong "salt bridge" interactions are detected by rigidity analysis and give this psychrophilic enzyme structure a signature of enhanced rigidity very similar to that of the thermophilic structures. Taken literally, this would indicate that AbCS would only operate at high temperatures, which cannot be physically correct. The discrepancy is resolved if hydrophobic tether interactions are treated as weaker constraints in rigidity analysis (as described in Methods) to take account of the cold conditions. Under these conditions, AbCS-2 now appears even less rigid than mesophilic PigCS-0, and has the flexibility it needs to operate under psychrophilic conditions.

Angular measures describing domain opening and closing in citrate synthase

To study the mobility of different CS structures, structural descriptors are required that are transferrable and comparable across structures and which capture the character of the open-to-closed transition involved in the mechanism of citrate synthase. Use is made of a four-atom measure based on the position of the C-α atoms of residues located at the tips and hinge bases of the small domains, as illustrated in Figure 2A. In a dimeric structure, four atoms (A,B,C,D) in the order tip-hinge-hinge-tip define two angles (ABC, BCD) and a dihedral angle (ABCD) describing the position of the small domain "flaps" relative to the main body of the dimer. The residues whose C-α atoms are used to define the tip and hinge base for each structure are given in Table II.

(Fig2)

(Table II)

In Figures 2B,C these angular measures are applied to describe a broad set of CS crystal structures, including the set of six open structures that were examined for flexible motion, and a corresponding set of closed structures. It is clear from Figure 2B that the angles ABC/BCD clearly differentiate the open structures from the closed, confirming that the angular measures are appropriate to describe the functional motion of CS. The dihedral measure ABCD (Figure 2C) shows more variation, although there is a tendency for more closed structures to show smaller (less negative) values of the dihedral. Clearly the range of angles explored by the open structures is wider than the narrow range seen in the closed structures.

Flexible motion along normal mode directions: angular description

To explore flexible motion we consider motion along the eigenvectors of low-frequency normal modes identified by elastic network modelling (see Methods). The normal mode analysis produces a set of six trivial rigid-body motions (with zero frequency) so the first non-trivial mode of motion is mode 7. Eigenvectors have been obtained from elastic network modelling [20] and explored using all-atom geometric simulations [21,22] for seven open input structures, from pig (PigCS-0), *Thermoplasma* (TaCS-0 and TaCS-1), *Pyrobaculum* (PaCS-0), *Bacillus* (BsCS-2), *Thermus* (TtCS-0), and *Sulfolobus* (SsCS-0). In all cases, modes involving motion of the small domains relative to the main body of the dimer appeared as the three lowest-frequency non-trivial normal modes: modes 7,8 and 9. In all cases, the mode 7 eigenvector describes an antisymmetric opening/closing mode in which the binding cleft on

one chain opens while the other closes. The mode 9 eigenvector describes a symmetric mode in which the two binding clefts open and close together. The character of the mode 8 eigenvector is far more variable between structures, and often involves larger variations of the dihedral. Physically, these eigenvectors were expected to form a basis set, with real flexible motion involving combinations of all three modes. Therefore, the range of flexible motion that is possible along each mode eigenvector was examined first, and then if necessary motion biased along linear combinations of mode eigenvectors was considered. Particular attention was paid to three cases in which matching open and closed crystal structures are available for comparison (pig, *Thermus*, and *Thermoplasma*).

(Fig3)

In Figure 3A,B motion of the open structure from pig (PigCS-0) is shown along normal modes 7,8,9 using our angular measures. Considering the angles ABC and BCD (Figure 3A), it is clear that mode 7 is an antisymmetric opening/closing motion, while in this case modes 8 and 9 are both symmetric closing motions. Considering also the dihedral ABCD (Figure 3B), it can be seen that modes 8 and 9 are distinguished by the behaviour of the dihedral angle. Motions with amplitudes of 20 to 30 degrees are possible in all directions from the input structure, indicating that the open structure is not an extremum of opening motion. Strikingly, the matching closed conformation (PigCS-2) lies almost exactly on the trajectory of closing motion along mode 9, even though no information about this closed structure was used in the simulation. The PigCS-2 conformation also lies well within the amplitude of flexible motion available to the PigCS-0 structure, indicating that the crystallographic closed structure containing bound ligands is not an extremum of closing motion without ligands present.

In Figure 3C,D the flexible motion of the open *Thermus* CS structure, TtCS-0, is shown. Once again, mode 7 is an antisymmetric motion, while modes 8 and 9 are both symmetric motions, differing in their dihedral character. Although the TtCS-0 structure is initially one of our most open structures, more open than PigCS-0 by about 15 degrees in the ABC and BCD angles, TtCS-0 is still not an extremum of opening motion and substantial amplitudes of motion are again possible in all directions. It can be seen from Figure 3D that the corresponding closed conformation, TtCS-2, lies between the trajectories of modes 8 and 9 in the space of our angular measures. Also shown is a trajectory of flexible motion along a constructed mode vector consisting of equal parts of the mode 8 and mode 9 eigenvectors. This trajectory passes almost exactly through the TtCS-2 data point, and can even close further (as was seen for PigCS) in the absence of bound ligands. The need for components of two modes rather than one to describe the closing motion in this case may simply reflect the very large scale of the closing motion for this enzyme.

(Fig4)

For *Thermoplasma* CS, the holoenzyme crystallised with oxaloacetate in the binding cleft (TaCS-1) was initially taken as a partly open input structure, while the corresponding closed structure was the enzyme crystallised with both oxaloacetate and citrate (TaCS-2). TaCS-1 is thus already close to being a closed structure, as is visible in the angular measures ABC, BCD. In Figure 4A,B flexible motions of the TaCS-1 structure are shown. The character of modes 7 and 9 are very similar to the case of PigCS-0, with one antisymmetric and one symmetric mode. The character of mode 8 is less clear from consideration of the ABC/BCD angles, but can be seen in Figure 4B to be predominantly a dihedral motion. The corresponding closed structure, TaCS-2, lies almost on the trajectory of flexible motion of

TaCS-1 along mode 9.

A more open CS structure from *Thermoplasma*, crystallised with no ligands bound (TaCS-0) was previously reported by Russell et al. [32] but not deposited in the PDB; coordinates were kindly provided to us by the authors. Examining its flexible motion, the characters of modes 7 (antisymmetric closing) and 9 (symmetric closing) were found to be very similar to the cases of PigCS-0 and TaCS-1. The character of mode 8, by contrast, differs considerably between TaCS-1 and TaCS-2. Trajectories for these flexible motions are shown in Figure 4C,D. We find that the conformations of both TaCS-1 and TaCS-2 lie very close, in our angular measures, to the trajectory of flexible motion of TaCS-0 along mode 9, a symmetric closing motion.

Flexible motion: structural comparisons

Open and closed CS structures from the same organism can be compared directly. Figure 5A shows a superposition of the open PigCS-0 and closed PigCS-2 dimeric structures, using a cartoon representation of the backbone and suppressing side chains for clarity. The central body of the dimer is clearly very similar between the structures, with the main difference being in the attitude of the two outer small domains. Figure 5B shows a superposition of the PigCS-2 structure with a frame from the trajectory of flexible motion of PigCS-0 along mode 9. The simulated symmetric closing motion has brought the small domains close to the observed PigCS-2 conformation.

(Fig5)

Since motion along mode 7 involves a closing motion in one cleft while the other opens, the

same comparison was made using a structure from the mode 7 trajectory, as shown in Figure 5C. In this case, the alignment of structures is carried out only on the closing chain (A) rather than on the entire dimer. Strikingly, the closing chain during motion along mode 7 also shows a close resemblance to the PigCS-2 structure, while the small domain of the other chain has diverged to a much more open position. It appears that the cleft closure involved in the functional motion of citrate synthase can be generated by an antisymmetric motion of the small domains as well as by the crystallographically-observed symmetric motion. Since the real dynamics in solution will include components of multiple low-frequency normal modes, this suggests the possibility of an independent cleft-closing motion, formed from the sum or the difference of the symmetric and antisymmetric motions.

According to our angular measures, the symmetric closure of the *Thermus* CS structure from TtCS-0 to TtCS-2 is described by a combination of modes 8 and 9 of TtCS-0. Figure 5D shows a superposition of the TtCS-0 and TtCS-2 crystal structures. Figure 5E compares TtCS-2 with a frame from the simulated motion of TtCS-0 along the closing mode "8+9", showing how well the modelled motion describes the closed structure. Due to the large scale of the closing motion we cannot in this case comment on asymmetric cleft closure involving mode 7.

For *Thermoplasma* CS, Figures 5F,G,H show a set of superpositions analogous to those for the pig structures. Panel 5F is an overlay of the open and closed crystal structures, TaCS-0 and TaCS-2. Panel 5G compares TaCS-2 with a frame from the motion of TaCS-0 along the symmetric closure mode 9, showing that the dimer has moved close to the TaCS-2 structure. Panel 5H shows a superposition using a frame from the motion of TaCS-0 along the antisymmetric mode 7, showing that the closing cleft is now similar to the TaCS-2 structure

while the opening cleft has diverged further. This indicates that in *Thermoplasma* CS, as in the pig CS, the functional motion of the enzyme may be achievable by independent closure of the binding clefts as well as by the crystallographically-observed symmetric closure.

Flexible motion: RMSD measures

The striking visual impression from the superpositions in Figure 5 can be quantified by measuring the C-α RMSD between the simulated structures during flexible motion and the reference open and closed structures. For symmetric motion, the relevant measure is the RMSD for the entire dimer. For antisymmetric (mode 7) motion, the binding cleft for one chain will be closing, and becoming more similar to the closed crystal structure, while the cleft for the other chain will be opening and becoming less similar to any crystal structure. In this case we consider the RMSD of only the closing chain (chain A).

(Fig6)

Figure 6A shows data for motion of PigCS-0 along modes 7 and 9. Motion along mode 9 takes the dimer from its starting point, coincident with PigCS-0, to a point about 3 Å distant from PigCS-0 and just over 1 Å distant from PigCS-2. This is clearly far more similar to the closed than to the input open structure. If a single closing chain is considered, however, modes 7 and 9 provide equally good descriptions of the closing motion. This suggests that the intrinsic capacity for flexible motion of the pig CS structure is as compatible with independent closing motions of the two binding clefts as it is with the symmetric closure directly observed in the crystallographic structures. This in turn implies that the symmetric closing motion implied by crystallography is only a subset of the true motion involved in function *in vivo*.

Figure 6B shows data from simulated motion beginning with the TtCS-0 structure along the constructed mode "8+9", which according to the angular measures represents the open-to-closed transition. RMSDs are given for frames from the simulation, measuring the similarity of the full dimer to the open input TtCS-0 and to the closed TtCS-2 structures. The RSMD between TtCS-2 and TtCS-0 is approximately 3.5 Å, while the simulations lead to a structure lying more than 3 Å distant from TtCS-0 and just over 1 Å distant from TtCS-2. The impression obtained from our angular description of the motion is thus confirmed.

Similarly, Figure 6C shows data for simulations based on the TaCS-1 structure moving along mode 9, with RMSD data measuring the distance of simulated frames from the TaCS-1 and TaCS-2 structures. In this case, the RMSD between TaCS-1 and TaCS-2 is very small to begin with, approximately 1.3 Å, making quantitative assessment difficult. However, the simulation clearly produces structures more similar to TaCS-2 than to the input TaCS-1 structure.

The more open TaCS-0 structure is slightly more distinct from TaCS-2, with an initial RMSD between the two of approximately 1.6 Å. In Figure 6D, RMSDs are compared to TaCS-0 and TaCS-2 for structures generated by the flexible motion of TaCS-0 along modes 7 and 9. The RMSD comparison is performed for the single closing chain (A) in mode 7, and for both the entire dimer and a single chain in mode 9. In both cases, structures are found that lie within 1 Å RMSD of the closed TaCS-2 structure.

These RMSD data confirm that the angular measures are giving an accurate picture of the character of the flexible motion in CS structures, and suggest that the crystallographically

observed symmetric closing motion is not the only functional motion intrinsic to the structure of citrate synthase.

Flexible motion and conservation of mode character

In the structures whose flexible motion has been discussed so far, a general similarity in the characters of mode 7 (an antisymmetric closing mode) and mode 9 (a symmetric closing mode) is observed. Mode 8, however, appears to have a different character in each case, and even differs noticeably between the very similar TaCS-0 and TaCS-1 structures.

(Fig7)

Figure 7 illustrates the character of flexible motion for all the "open" structures, using our angular measures. Mode 7, shown in Figures 7A,B, has an antisymmetric opening/closing character in all cases; the behaviour of the *Pyrobaculum* CS structure (PaCS-0) differs slightly from the rest of the dataset in its dihedral character (Figure 7B). The character of mode 8 (Figure 7C,D) is highly variable between structures. Mode 9, by contrast, is in every case a symmetric opening/closing motion (Figure 7E) with very similar dihedral behaviour (Figure 7F), essentially describing the distribution in angular space of the open and closed crystal structures as seen in Figure 2B,C.

CONCLUSION

We have been able, using rapid, physically simplified all-atom methods [22], to examine the flexibility and rigidity of a wide variety of CS structures in parallel. Our results are consistent with crystallographic structural data on the CS open/closed transition and also display intriguing features that are implicit in the structural data but only become visible through modelling. Direct comparison of our data with simulations at a higher level of theory, i.e. MD, is not easy; due to the large size of the dimeric CS structure, MD investigations have tended to explore relatively short trajectories on the order of 1ns in duration [11-13,33]. One MD study has suggested some capacity for spontaneous open/closed transition motions in the unliganded protein [12], while a subsequent study using essential dynamics sampling found that the transition jammed when targeted along the transition direction [33] in short (500ps) trajectories.

Rigidity analysis shows a signature for thermostabilisation by increased rigidity in thermophilic CS structures, visible particularly at cut-off energies around 0.5 to 1.0 kcal/mol, the "room temperature" range. This complements the finding of enhanced "folding core" stability [7] in thermostable enzymes and of a "corresponding states" relationship between the rigidity of mesophilic enzymes at room temperature and thermophilic enzymes at high temperatures[8]. The stabilisation of psychrophilic AbCS-2 by strong polar (salt bridge/ion pair) interactions appears at first sight to produce a similar rigidification. However, when the hydrophobic interaction is reduced in its rigidifying effect, as is appropriate to the cold Antarctic environment, AbCS-2 no longer appears excessively rigid and we instead see a reduced rigidity in the cold-adapted structure, complementing the enhanced rigidity of the heat-adapted structures, consistent with the hypothesis of corresponding states. Our results

are consistent with MD results reporting greater flexibility in cold-adapted CS [11] and greater stability in thermophilic CS structures [13].

The four-atom angle and dihedral measures describe the attitude of the small domains relative to the body of the dimer and provide a transferrable measure of openness/closedness describing a wide range of citrate synthase crystal structures. This allows us to discuss the character of flexible motion in multiple CS structures on a common basis. As expected [2,3,20] we find that the low-frequency normal mode eigenvectors obtained from elastic network modelling of CS structures provide a good description of binding-site cleft opening/closing motions.

According to our geometric simulations, CS structures are generally capable of opening further than is observed crystallographically. They are likewise capable of closing further in the absence of bound ligands than is observed in ligand-bound crystal structures, consistent with MD results [12]. This suggests that observed open and closed structures are those selected by crystallisation conditions and ligand binding from a wide range of structures explored in solution by flexible motion.

The set of structures studied shows conservation of an antisymmetric mode (7) and a symmetric mode (9). Mode 8 is far more variable in its character. In cases with matching open/closed structures, crystallographic open-to-closed transitions are well described by symmetric closing motion based on mode 9 or a combination involving mode 9. The character of the lowest-frequency non-trivial normal modes, especially a symmetric opening/closing mode appearing as mode 9, is well conserved across mesophilic and extremophilic CS structures from the three domains of life – eukarya, bacteria and archaea.

That is, the constraint-network changes involved in thermostabilisation do not alter the functional cleft-closing motion. It is plausible that conservation of specific intrinsic flexibility in the structure is itself a constraint on the evolution of citrate synthase, as the loss or alteration of the flexible modes involved in function would reduce or destroy the effectiveness of the enzyme.

The results for pig and *Thermoplasma* CSs suggest that the opening and closing of the two reaction sites of the dimer can occur either together or separately, through both symmetric and antisymmetric closing modes of motion. The outcome of an MD study using essential dynamics sampling [33], in which motion biased along the symmetric closing direction led to jamming rather than to a full open-to-closed transition trajectory, is now understandable if antisymmetric and independent motions are also important to CS dynamics. We would not expect the antisymmetric or independent functional motions to be directly evidenced by crystallography, as crystallisation will naturally tend to produce doubly-open or doubly-closed structures. However, the capacity for non-symmetric motion is intrinsic to the CS structure and is brought out by our simulation study, illustrating the value of modelling to access all the information implicit in crystal structure data.

REFERENCES

1. Delarue M, Dumas P. On the use of low-frequency normal modes to enforce collective movements in refining macromolecular structural models. Proceedings of the National Academy of Sciences of the United States of America 2004;101(18):6957-6962.
2. Marques O, Sanejouand YH. Hinge-bending motion in citrate synthase arising from normal mode calculations. Proteins 1995;23(4):557-560.
3. Tama F, Sanejouand YH. Conformational change of proteins arising from normal mode calculations. Protein engineering 2001;14(1):1-6.
4. Daniel RM, Danson MJ, Hough DW, Lee CK, Peterson ME, Cowan DA. Enzyme stability and activity at high temperatures. In: Thomas KSST, editor. Protein Adaptation in Extremophiles, Molecular Anatomy and Physiology of Proteins New York: Nova Science Publishers; 2008. p 1-34.
5. Bell GS, Russell RJ, Connaris H, Hough DW, Danson MJ, Taylor GL. Stepwise adaptations of citrate synthase to survival at life's extremes. From psychrophile to hyperthermophile. European journal of biochemistry / FEBS 2002;269(24):6250-6260.
6. Howell SC, Inampudi KK, Bean DP, Wilson CJ. Understanding Thermal Adaptation of Enzymes through the Multistate Rational Design and Stability Prediction of 100 Adenylate Kinases. Structure 2013:218-229.
7. Rader AJ. Thermostability in rubredoxin and its relationship to mechanical rigidity. Phys Biol 2010;7(1).
8. Radestock S, Gohlke H. Protein rigidity and thermophilic adaptation. Proteins 2011;79(4):1089-1108.

9. van der Kamp MW, Shaw KE, Woods CJ, Mulholland AJ. Biomolecular simulation and modelling: status, progress and prospects. Journal of the Royal Society, Interface / the Royal Society 2008;5 Suppl 3:S173-190.

10. van der Kamp MW, Mulholland AJ. Combined quantum mechanics/molecular mechanics (QM/MM) methods in computational enzymology. Biochemistry 2013;52(16):2708-2728.

11. Spiwok V, Lipovova P, Skalova T, Duskova J, Dohnalek J, Hasek J, Russell NJ, Kralova B. Cold-active enzymes studied by comparative molecular dynamics simulation. Journal of molecular modeling 2007;13(4):485-497.

12. Roccatano D, Mark AE, Hayward S. Investigation of the mechanism of domain closure in citrate synthase by molecular dynamics simulation. Journal of molecular biology 2001;310(5):1039-1053.

13. Cordeiro JMM. Dynamics of meso and thermo citrate synthases with implicit solvation. Int J Quantum Chem 2006;106(3):652-658.

14. Saunders MG, Voth GA. Coarse-graining methods for computational biology. Annual review of biophysics 2013;42:73-93.

15. Stansfeld PJ, Sansom MS. Molecular simulation approaches to membrane proteins. Structure 2011;19(11):1562-1572.

16. Hall BA, Chetwynd AP, Sansom MS. Exploring peptide-membrane interactions with coarse-grained MD simulations. Biophysical journal 2011;100(8):1940-1948.

17. Hespenheide BM, Rader AJ, Thorpe MF, Kuhn LA. Identifying protein folding cores from the evolution of flexible regions during unfolding. Journal of Molecular Graphics & Modelling 2002;21(3):195-207.

18. Jacobs DJ, Rader AJ, Kuhn LA, Thorpe MF. Protein flexibility predictions using graph theory. Proteins 2001;44(2):150-165.

19. Wells SA, Jimenez-Roldan JE, Roemer RA. Comparative analysis of rigidity across protein families. Phys Biol 2009;6(4).

20. Suhre K, Sanejouand YH. ElNemo: a normal mode web server for protein movement analysis and the generation of templates for molecular replacement. Nucleic acids research 2004;32(Web Server issue):W610-614.

21. Wells SA, Menor S, Hespenheide B, Thorpe MF. Constrained geometric simulation of diffusive motion in proteins. Phys Biol 2005;2(4):S127-S136.

22. Jimenez-Roldan JE, Freedman RB, Romer RA, Wells SA. Rapid simulation of protein motion: merging flexibility, rigidity and normal mode analyses. Phys Biol 2012;9(1):016008.

23. Ahmed A, Rippmann F, Barnickel G, Gohlke H. A Normal Mode-Based Geometric Simulation Approach for Exploring Biologically Relevant Conformational Transitions in Proteins. Journal of Chemical Information and Modeling 2011;51(7):1604-1622.

24. Kruger DM, Ahmed A, Gohlke H. NMSim web server: integrated approach for normal mode-based geometric simulations of biologically relevant conformational transitions in proteins. Nucleic acids research 2012;40(Web Server issue):W310-316.

25. Farrell DW, Speranskiy K, Thorpe MF. Generating stereochemically acceptable protein pathways. Proteins-Structure Function and Bioinformatics 2010;78(14):2908-2921.

26. Amin NT, Wallis AK, Wells SA, Rowe ML, Williamson RA, Howard MJ, Freedman RB. High-resolution NMR studies of structure and dynamics of human ERp27 indicate extensive interdomain flexibility. The Biochemical journal 2013;450(2):321-332.

27. Li H, Wells SA, Jimenez-Roldan JE, Romer RA, Zhao Y, Sadler PJ, O'Connor PB. Protein flexibility is key to cisplatin crosslinking in calmodulin. Protein science : a publication of the Protein Society 2012;21(9):1269-1279.

28. Chen VB, Arendall WB, 3rd, Headd JJ, Keedy DA, Immormino RM, Kapral GJ, Murray LW, Richardson JS, Richardson DC. MolProbity: all-atom structure validation for macromolecular crystallography. Acta crystallographica Section D, Biological crystallography 2010;66(Pt 1):12-21.

29. Schrodinger, LLC. The PyMOL Molecular Graphics System, Version 1.3r1. 2010.

30. Moore V, Kanu A, Byron O, Campbell G, Danson MJ, Hough DW, Crennell SJ. Contribution of inter-subunit interactions to the thermostability of Pyrococcus furiosus citrate synthase. Extremophiles 2011;15(3):327-336.

31. Russell RJ, Gerike U, Danson MJ, Hough DW, Taylor GL. Structural adaptations of the cold-active citrate synthase from an Antarctic bacterium. Structure 1998;6(3):351-361.

32. Russell RJ, Hough DW, Danson MJ, Taylor GL. The crystal structure of citrate synthase from the thermophilic archaeon, Thermoplasma acidophilum. Structure 1994;2(12):1157-1167.

33. Daidone I, Roccatano D, Hayward S. Investigating the accessibility of the closed domain conformation of citrate synthase using essential dynamics sampling. Journal of molecular biology 2004;339(3):515-525.

ACKNOWLEDGMENTS

Author contributions: SJC and MJD selected structures for the study and identified tip and hinge residues. SAW carried out rigidity analysis and geometric simulation, extracted angular

and RMSD measures, and prepared graphics. All authors collaborated on the interpretation of results and the preparation of the manuscript.

FIGURE LEGENDS

Figure 1

Structure and rigidity of dimeric citrate synthase. Panel (A): rigid cluster decomposition (RCD) of open pig citrate synthase (PigCS-0) at a hydrogen-bond energy cut-off of 0.0 kcal/mol. The largest rigid clusters are shown in cartoon rendering and coloured as a rainbow from red (largest rigid cluster) to blue. Flexible regions of the backbone not lying in a large rigid cluster are shown as faint grey ribbon. Side-chains have been suppressed for clarity. Panel (B): corresponding rigid cluster decomposition (RCD) of open *Thermus* citrate synthase (TtCS-0) at a hydrogen-bond energy cut-off of 0.0 kcal/mol. Panel (C): RCD of PigCS-0 at a hydrogen-bond energy cut-off of -1.0 kcal/mol. Panel (D): RCD of TtCS-0 at a hydrogen-bond energy cut-off of -1.0 kcal/mol. Panel (E): RCD of PigCS-0 at a hydrogen-bond energy cut-off of -2.0 kcal/mol. Panel (F): RCD of TtCS-0 at a hydrogen-bond energy cut-off of -2.0 kcal/mol. Panel (G): the rigidity fraction, f_i, of backbone atoms lying in the i largest rigid clusters, as a function of cut-off energy E and index i, for structures from mesophilic (pig; PigCS-0: open red circle) and extremophilic (*Thermus*; TtCS-0: open black square) organisms. A line is drawn through the f_5 points in each data set for clarity. Panel (H): rigidity fraction, f_5, as a function of cut-off energy for structures from mesophilic (pig: PigCS-0, closed red circles), thermophilic (*Thermoplasma:* TaCS-1, green cross, *Pyrobaculum:* PaCS-2, blue cross, *Thermus:* TtCS-0, black square, *Pyrococcus:* PfCS-2, open grey triangle) and psychrophilic (*Arthrobacter:* AbCS-2) organisms. For AbCS-2, traces are shown for conventional rigidity analysis as open black diamonds, and for analysis with weaker hydrophobic interactions as closed black diamonds.

Figure 2

Three-atom angles and four-atom dihedral angles describe the conformational state of

dimeric citrate synthase. Panel (A): definition of angular measures based on α-carbon atoms in four key residues. Two angles and a dihedral angle are defined by residues lying at the tips and bases of the small domains. Panel (B): angular disposition of small domains for a variety of CS crystal structures. Open structures lie at higher values of the angles ABC, BCD, while closed structures lie at smaller angular values (<80 degrees). Open structures are shown: PigCS-0 (open red triangle), TtCS-0 (open green triangle), TaCS-0 (open blue circle) and TaCS-1 (closed blue circle), with PaCS-0, BsCS-2 and SsCS-0 (black crosses). Closed structures are shown: PigCS-2 (closed red triangle), TtCS-0 (closed green triangle), TaCS-2 (closed blue diamond), with PfCS-2 and AbCS-2 (black crosses). Panel (C): angular disposition of small domains, including dihedral angle ABCD. In panels B and C, a red ellipse highlights the closed crystal structures.

Figure 3

Variation of the cleft opening angles ABC, BCD (two-D plots) and of the dihedral angle ABCD (three-D plots) during flexibility simulations. We explore low-frequency modes 7 (red crosses), 8 (green crosses), and 9 (blue asterisks) in open CS structures from pig and *Thermus*. Panels (A) and (B) flexible motion around the PigCS-0 structure (open red triangle), with a data point (closed red triangle) for the closed structure PigCS-2. Panel (C) and (D): variation of the angles ABC, BCD (c) and of the dihedral angle ABCD (d) during flexibility simulations exploring low-frequency modes 7,8,9 around the structure of TtCS-0 (open green triangle) from *Thermus*, and a data point (closed green triangle) for the matching "closed" structure TtCS-2. A trajectory is also shown in panel (D) for a constructed mode consisting of equal contributions of modes 8 and 9 (black crosses).

Figure 4

Variation of the cleft opening angles ABC, BCD (two-D plots) and of the dihedral angle ABCD (three-D plots) during flexibility simulations. We explore low-frequency modes 7 (red crosses), 8 (green crosses), and 9 (blue asterisks) in open CS structures from *Thermoplasma*. Panels (A) and (B): variation of the angles ABC, BCD (A) and of the dihedral angle ABCD (B) during flexibility simulations exploring low-frequency modes 7,8,9 around the partially-open structure TaCS-1 (closed blue circle) from *Thermoplasma*, with data points for the matching closed structure TaCS-2 (closed blue diamond) and for the fully-open structure TaCS-0 (open blue circle). Panels (C) and (D): variation of the angles ABC, BCD (C) and of the dihedral angle ABCD (D) during flexibility simulations exploring low-frequency modes 7,8,9 around the open structure TaCS-2 from *Thermoplasma*, with data points for the matching closed structure TaCS-2 and for the partially-open structure TaCS-1.

Figure 5

Structural superpositions illustrating the closing motion of CS. Structures as observed in crystallography (A,D,F) and in flexible motion simulations (B,C,E,G,H).

(A) structural alignment of open (PigCS-0, light grey cartoon) and closed (PigCS-2, black cartoon) CS crystal structures from pig. The superposed red ellipse highlights the motion of the small domain in closing the active site cleft.

(B) structural alignment of a frame from simulated motion of PigCS-0 along low-frequency mode 9 (light grey cartoon) and the closed PigCS-2 structure (black cartoon).

(C) structural alignment of a frame from simulated motion of PigCS-0 along low-frequency mode 7 (light grey cartoon) and the closed PigCS-2 structure (black cartoon). In this case the alignment is performed on chain A only, at left. The superposed yellow box highlights the further opening of the active site cleft in the other chain.

(D) structural alignment of open (TtCS-0, light grey cartoon) and closed (TtCS-2, black

cartoon) CS crystal structures from *Thermus*.

(E) structural alignment of a frame from simulated motion of TtCS-0 along a constructed low-frequency mode "8+9" (light grey cartoon) and the closed TtCS-2 structure (black cartoon).

(F) structural alignment of open (TaCS-0, light grey cartoon) and closed (TaCS-2, black cartoon) CS crystal structures from *Thermoplasma*.

(G) structural alignment of a frame from simulated motion of TaCS-0 along low-frequency mode 9 (light grey cartoon) and the closed TaCS-2 structure (black cartoon).

(H) structural alignment of a frame from simulated motion of TaCS-0 along low-frequency mode 7 (light grey cartoon) and the closed TaCS-2 structure (black cartoon). In this case the alignment is performed on chain A, at left.

Figure 6

C-α RMSD comparisons between simulation frames and open (input) and closed CS structures during simulations of flexible motion. Each trace begins at x=0, in a state identical to the open input structure, and proceeds to the right, as indicated by the superposed arrow. Data points lying below the diagonal line on each plot indicate structures more similar to the closed than to the open structure.

(A) pig: flexible motion from PigCS-0 input compared to PigCS-0 and PigCS-2 crystal structures. Comparisons are shown for the entire dimer in motion along mode 9 (blue asterisks), and for chain A alone during motion of the dimer along mode 7 (red crosses) and mode 9 (blue open circles).

(B) *Thermus*: flexible motion from TtCS-0 input compared to TtCS-0 and TtCS-2 crystal structures, during motion of the dimer along the constructed mode 8+9.

(C) *Thermoplasma*: flexible motion from TaCS-1 input compared to TaCS-1 and TaCS-2 crystal structures, during motion of the dimer along mode 9.

(D) *Thermoplasma*: flexible motion from TaCS-0 input compared to TaCS-0 and TaCS-2 crystal structures. Comparisons are shown for the entire dimer in motion along mode 9 (blue asterisks), and for chain A alone during motion of the dimer along mode 7 (red crosses) and mode 9 (blue open circles).

Figure 7

Angular character of motion along low-frequency modes 7, 8 and 9 for a range of open CS input structures. Two-dimensional plots show variations of the cleft opening angles ABC, BCD; three-dimensional plots also show variation of the dihedral angle ABCD.

(A) and (B): character of low-frequency mode 7 as described by angle-angle (A) and angle-angle-dihedral (B) measures.

(C) and (D): character of low-frequency mode 8 as described by angle-angle (C) and angle-angle-dihedral (D) measures.

(E) and (F): character of low-frequency mode 9 as described by angle-angle (E) and angle-angle-dihedral (F) measures.

TABLES

Table II

The PDB codes and identifying prefixes for the structures used in this study, the resolution in Angstroms at which each structure was determined, and ligands bound.

Table II

Amino acid residues used to define the angle and dihedral measurements in the CS structures, with values obtained from crystal structures for angles ABC, BCD and dihedral angle ABCD in degrees.

TABLE I

Organism and optimal growth temperature	**Prefix**	**PDB codes and resolutions (Angstroms) by number of ligands**		
		0	**1**	**2**
Sus scrofa (Pig) (37°C)	PigCS	3ENJ (1.78)	-	2CTS (2.00)
Thermus thermophilus (70°C)	TtCS	1IOM (1.50)	-	1IXE (2.30)
Thermoplasma acidophilum (59°C)	TaCS	*TaCS-0 ()	2IFC (1.70)	2R9E (1.95)
Sulfolobus solfataricus (80°C)	SsCS	1O7X (2.70)	-	-
Pyrobaculum aerophilum (100°C)	PaCS	2IBP (1.60)	-	
Bacillus subtilis (25°C)	BsCS	-	-	**2C6X (3.40)
Pyrococcus furiosus (100°C)	PfCS	-	-	1AJ8 (1.90)
Arthrobacter DS2-3R (0-10°C)	AbCS	-	-	1A59 (2.09)

*Not deposited in PDB; reported in [32]

** crystallised in open form; CoA ligand not in functional binding position

TABLE II

Structure	Tip residue	Hinge residue	ABC	BCD	ABCD
PigCS-0 : 3ENJ	G312	G386	83.3	83.3	-101.1
PigCS-1 : 2CTS			72.6	72.6	-83.3
TaCS-1 : 2IFC	G253	G328	78.7	82.8	-91.6
TaCS-2 : 2R9E			67.7	66.7	-93.5
TaCS-0			87.0	84.6	-101.5
TtCS-0 : 1IOM	K350	G323	97.5	97.5	-109.7
TtCS-2 : 1IXE			72.9	72.1	-103.5
BsCS-2 : 2C6X	G244	D318	99.9	100.2	-114.4
PaCS-0 : 2IBP	P279	G357	89.9	87.7	-117.1
SsCS-0 : 1O7X	K250	G324	93.1	93.7	-111.0
PfCS-2 : 1AJ8	K254	K323	70.9	71.1	-99.4
AbCS-2 : 1A59	K261	G331	73.4	73.4	-98.1

FIGURE 1

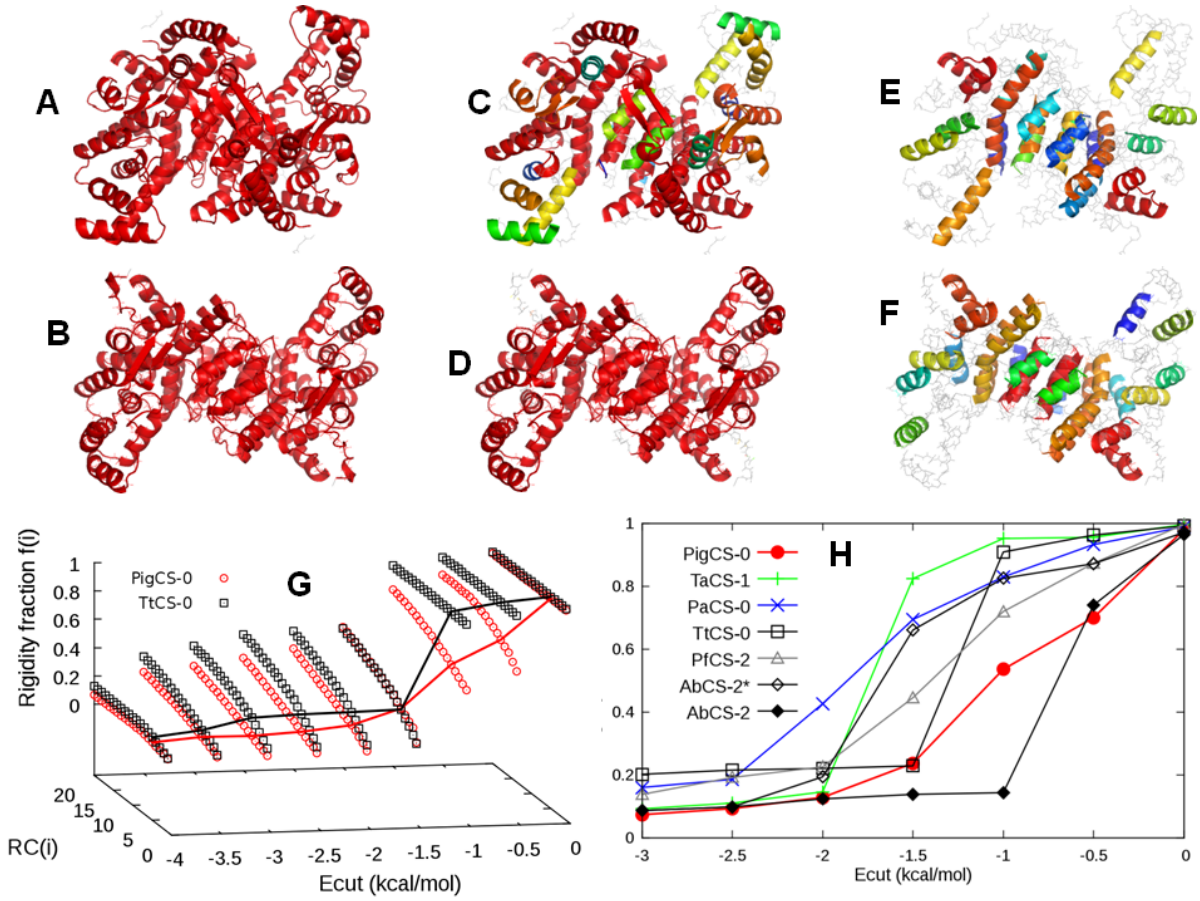
A
B
C
D
E
F
G
PigCS-0
TtCS-0
Rigidity fraction f(i)
RC(i)
Ecut (kcal/mol)
H
PigCS-0
TaCS-1
PaCS-0
TtCS-0
PfCS-2
AbCS-2*
AbCS-2
Ecut (kcal/mol)

FIGURE 2

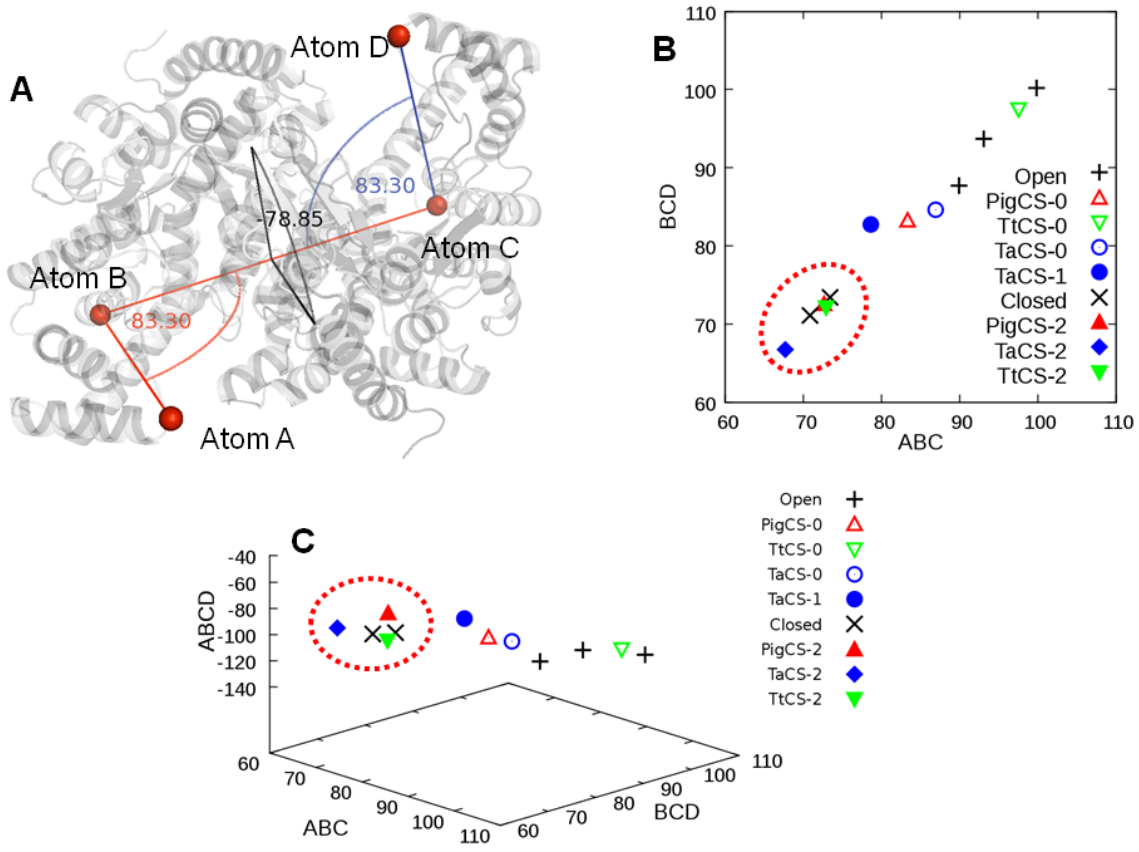
A
Atom D
83.30
-78.85
Atom C
Atom B
83.30
Atom A
B
BCD
ABC
Open
PigCS-0
TtCS-0
TaCS-0
TaCS-1
Closed
PigCS-2
TaCS-2
TtCS-2
C
ABCD
ABC
BCD

FIGURE 3

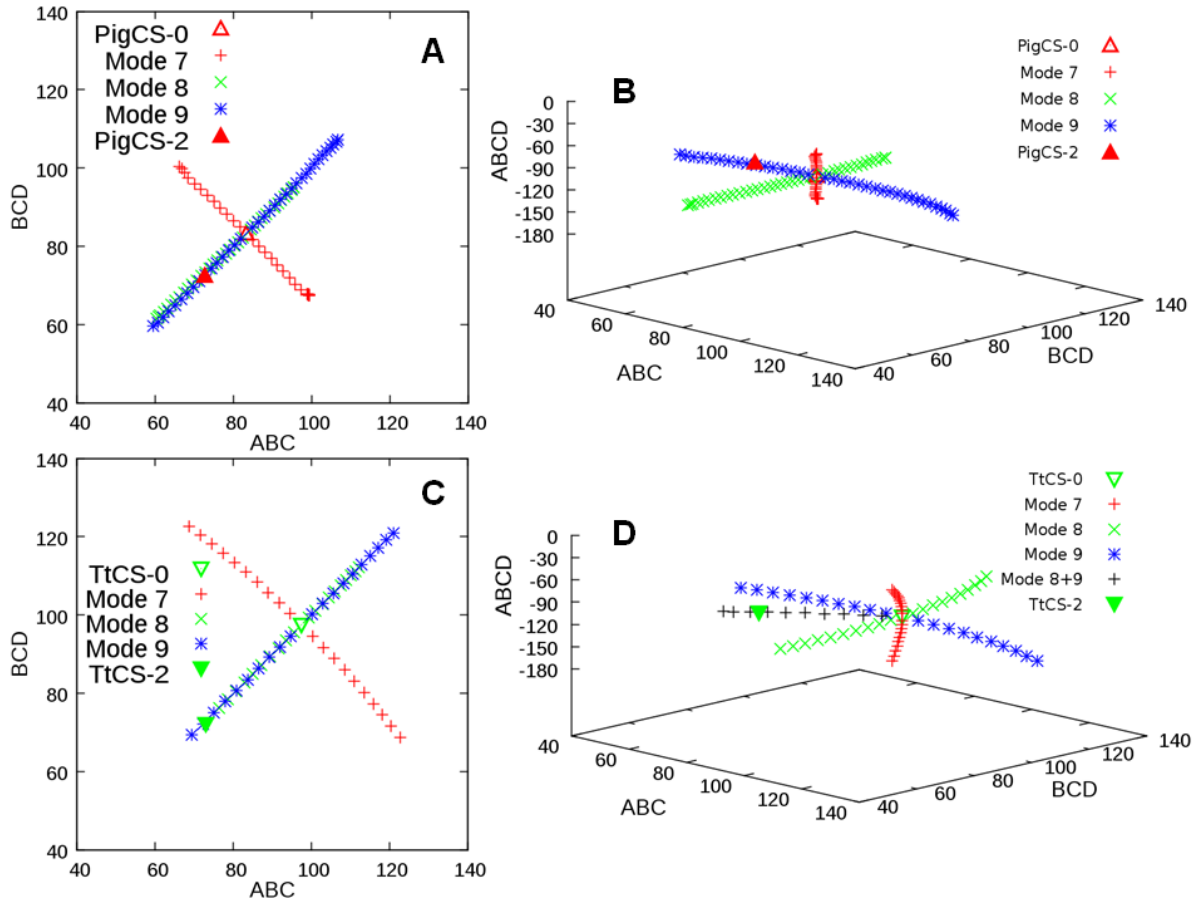
A
PigCS-0
Mode 7
Mode 8
Mode 9
PigCS-2
BCD
ABC
B
PigCS-0
Mode 7
Mode 8
Mode 9
PigCS-2
ABCD
ABC
BCD
C
TtCS-0
Mode 7
Mode 8
Mode 9
TtCS-2
BCD
ABC
D
TtCS-0
Mode 7
Mode 8
Mode 9
Mode 8+9
TtCS-2
ABCD
ABC
BCD

FIGURE 4

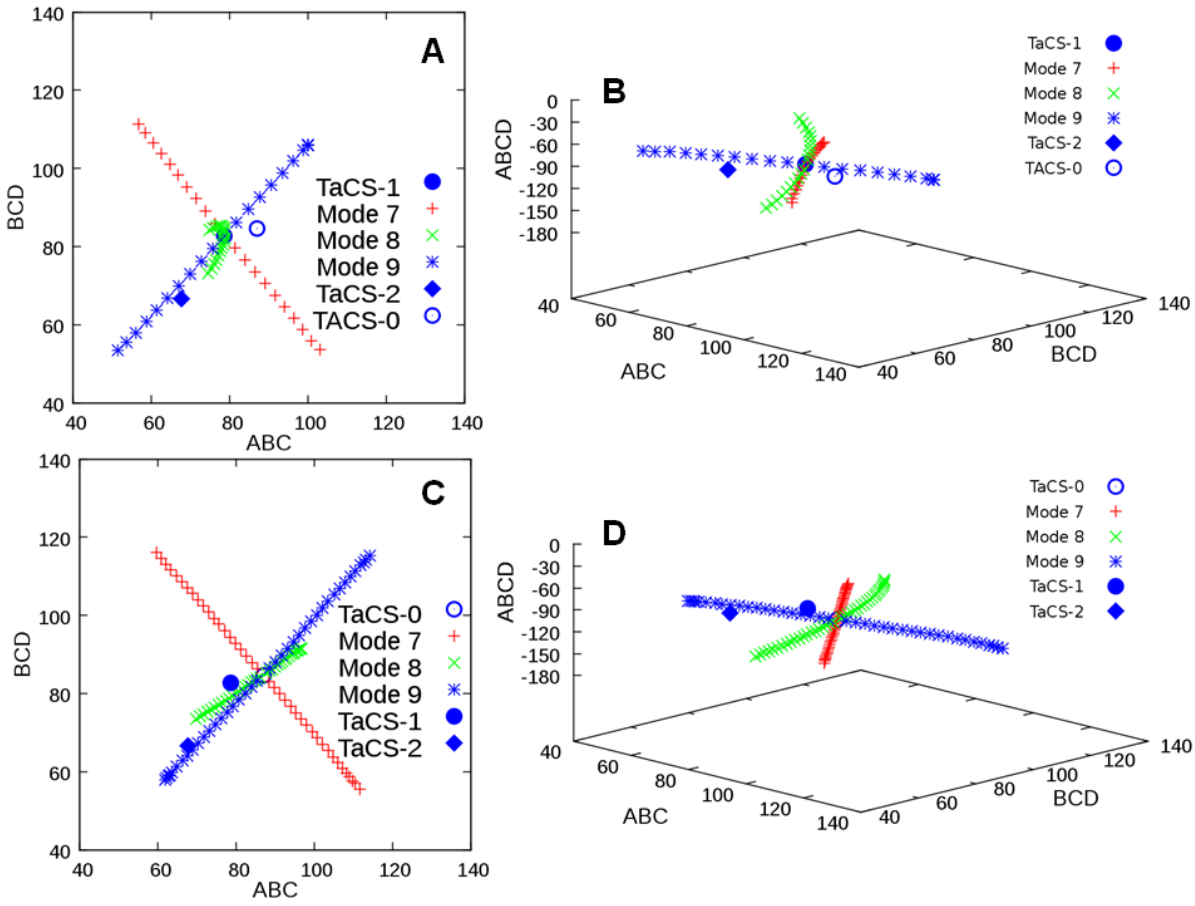
A
BCD
ABC
TaCS-1
Mode 7
Mode 8
Mode 9
TaCS-2
TACS-0
B
ABCD
ABC
BCD
TaCS-1
Mode 7
Mode 8
Mode 9
TaCS-2
TACS-0
C
BCD
ABC
TaCS-0
Mode 7
Mode 8
Mode 9
TaCS-1
TaCS-2
D
ABCD
ABC
BCD
TaCS-0
Mode 7
Mode 8
Mode 9
TaCS-1
TaCS-2

FIGURE 5

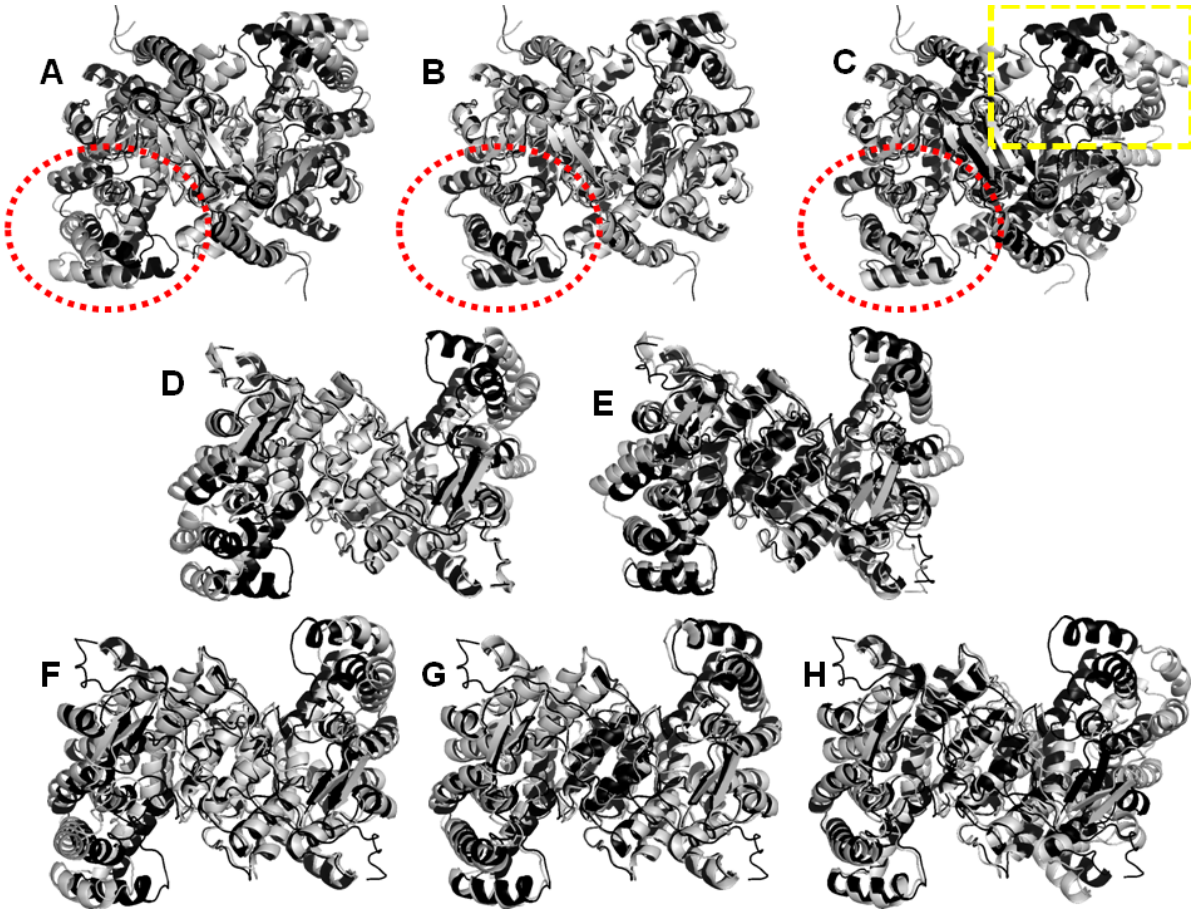

FIGURE 6

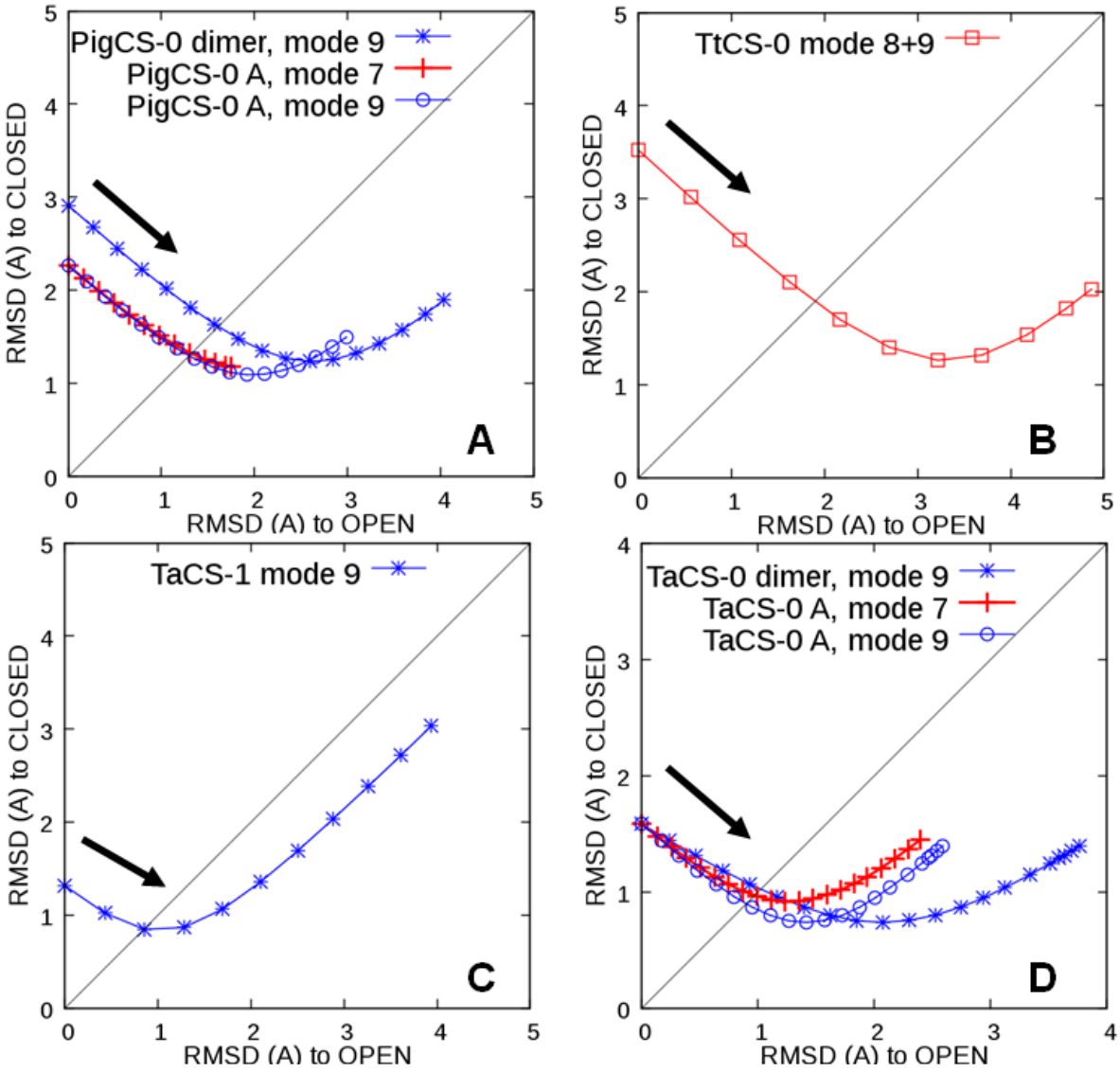
PigCS-0 dimer, mode 9
PigCS-0 A, mode 7
PigCS-0 A, mode 9
RMSD (A) to CLOSED
RMSD (A) to OPEN
A
TtCS-0 mode 8+9
B
TaCS-1 mode 9
C
TaCS-0 dimer, mode 9
TaCS-0 A, mode 7
TaCS-0 A, mode 9
D

FIGURE 7

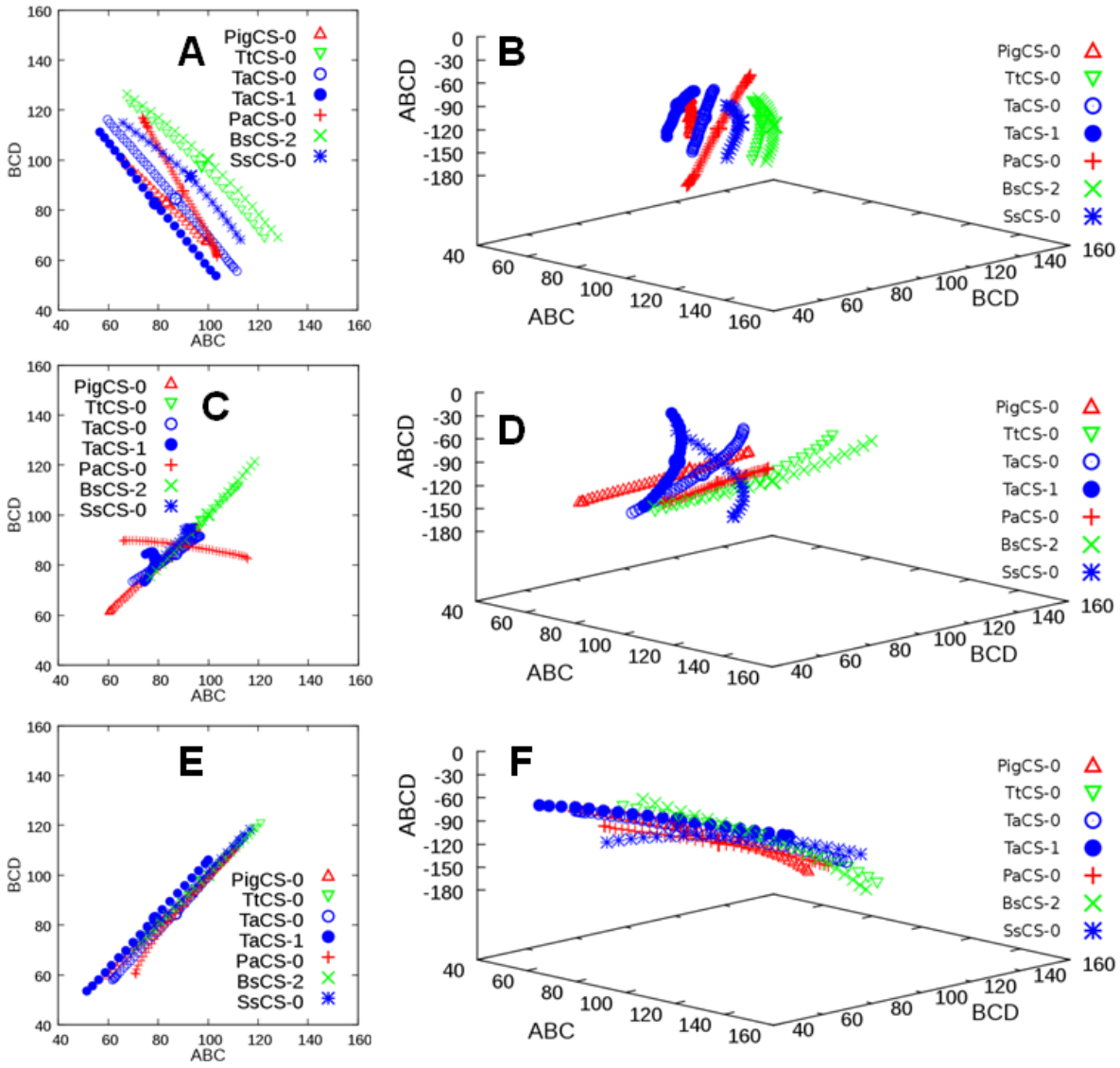
A
B
C
D
E
F
PigCS-0
TtCS-0
TaCS-0
TaCS-1
PaCS-0
BsCS-2
SsCS-0
ABC
BCD
ABCD